*Astronomy & Astrophysics* manuscript no. aa15306˙final
September 20, 2010

© ESO 2010

arXiv:1009.3392v1 [astro-ph.SR] 17 Sep 2010

# Deep *XMM-Newton* observation of the Eta Chamaleontis cluster⋆

J. López-Santiago[1], J. F. Albacete Colombo[2], and M. A. López-García[1]

[1] Departamento de Astrofísica y Ciencias de la Atmósfera, Universidad Complutense de Madrid, E-28040 Madrid, Spain
e-mail: `jls@astrax.fis.ucm.es; mal@astrax.fis.ucm.es`
[2] Centro Universitario Regional Zona Atlántica (CURZA) Universidad Nacional del COMAHUE, Monseñor Esandi y Ayacucho (8500), Viedma (Rio Negro), Argentina.
e-mail: `donfaca@gmail.com`

Received ...; accepted ...

## ABSTRACT

*Context.* The members of the $\eta$ Chamaleontis cluster are in an evolutionary stage in which disks are rapidly evolving. It also presents some peculiarities, such as the large fraction of binaries and accretion disks, probably related with the cluster formation process. Its proximity makes this stellar group an ideal target for studying the relation between X-ray emission and those stellar parameters.
*Aims.* The main objective of this work is to determine general X-ray properties of the cluster members in terms of coronal temperature, column density, emission measure, X-ray luminosity and variability. We also aim to establish the relation between the X-ray luminosity of these stars and other stellar parameters, such as effective temperature, binarity, and presence of accretion disks. Finally, a study of flare energies for each flare event detected during the observations and their relation with some stellar parameters is also performed.
*Methods.* We used proprietary data from a deep *XMM-Newton* EPIC observation pointed at the core of the $\eta$ Chamaleontis cluster. Specific software for the reduction of *XMM-Newton* data was used for the analysis of our observation. For the detection of sources in the composed EPIC pn+mos image, we used the wavelet-based code *PWDetect*. General coronal properties were derived from plasma model fitting. X-ray light curves in the 0.3–8.0 keV energy range were generated for each star.
*Results.* We determined coronal properties and variability of the $\eta$ Chamaleontis members in the *XMM-Newton* EPIC field-of-view. A total of six flare-like events were clearly detected in five different stars. For them, we derived coronal properties during the flare events and pseudo-quiescent state separately. In our observations, stars that underwent a flare event have higher X-ray luminosities in the pseudo-quiescent state than cluster members with similar spectral type with no indications of flaring, independently whether they have an accretion disk or not. Observed flare energies are typical of both pre-main- and main-sequence M stars. We detected no difference between flare energies of stars with and without an accretion disk.

**Key words.** Galaxy: open clusters and associations: individual ($\eta$ Chamaleontis) – stars: pre-main sequence – stars: coronae – stars: flare – X-ray: stars

## 1. Introduction

The $\eta$ Chamaleontis cluster (hereafter $\eta$ Chamaleontis), named after the eponymous B8V star $\eta$ Cha, was discovered by Mamajek et al. (1999) using *ROSAT* data. The authors proposed 13 members, twelve of them being X-ray sources. Later, they investigated main properties of the sources (Mamajek et al. 2000) and established a connection between the $\eta$ Chamaleontis cluster and the $\epsilon$ Chamaleontis stellar association (Frink et al. 1998). They are part of a number of nearly coeval stellar groups that includes the TW Hya association and that probably had their origin in the molecular complex Scorpius-Centaurus (see Mamajek et al. 2000). Its proximity and low stellar density converts the $\eta$ Chamaleontis in an unique scenario in the solar vicinity.

With an age of 6–8 Myr, $\eta$ Chamaleontis presents some particularities. Its members are in an evolutionary stage in which disks are rapidly evolving (see Table 1) and can provide further constraints on inner disk lifetimes (Haisch et al. 2005). It has been found that several cluster members are in fast transition from classical T-Tauri stars (CTTS-like) to debris disks (Megeath et al. 2005; Sicilia-Aguilar et al. 2009). Besides, the binary fraction observed in the cluster is twice higher than that found for field stars and dense clusters (Lyo et al. 2004), but similar to the binary fraction in Taurus. This result may suggest that there is a relation between the binary fraction and the stellar density of star-forming regions. Some studies of the Initial Mass Function (IMF) of $\eta$ Chamaleontis (e.g. Moraux et al. 2007) reveal that the cluster mass function shows a deficit of low mass stars and brown dwarfs. Nevertheless, Luhman (2004) indicates that other low-mass star-forming regions as Taurus have very few or none brown dwarfs in stellar samples of the size of $\eta$ Chamaleontis. However, the deficit of low mass stars in the cluster is still not well-known. Moraux et al. (2007), using numerical simulations, concluded that the IMF is typical of clusters formed from a compact configuration and that dynamical interactions can result in the lost of the original cluster members. For the age of $\eta$ Chamaleontis, those stars ejected in the early phases of the cluster formation might reach distances of 6 to 10 pc from the cluster center. Thus, one should look for these ejected members at angular distances up to 5 degrees from the core of the cluster. This scenario has been recently validated by Murphy et al. (2010), who identified four new probable cluster members and three possible members. With this new four stars,

---

⋆ This publication makes use of data products from the Two Micron All Sky Survey, which is a joint project of the University of Massachusetts and the Infrared Processing and Analysis Center/California Institute of Technology, funded by the National Aeronautics and Space Administration and the National Science Foundation.

**Table 1.** Spectral type, binarity and disk properties of $\eta$ Chamaleontis members in the XMM-Newton field of view.

| Source | RECX | Sp.T.$^{*}$ | Binarity$^{**}$ | Disk type$^{\dagger}$ | log $L_{\rm bol}$$^{\ddagger}$ (erg s$^{-1}$) |
|---|---|---|---|---|---|
| $\eta$ Cha | 2 | B8 | ? | debris | 35.5 |
| EH Cha | 3 | M3 | | TO | 32.7 |
| EI Cha | 4 | M1 | | TO | 32.9 |
| EK Cha | 5 | M4 | | TO | 32.6 |
| EL Cha | 6 | M3 | | | 32.7 |
| EM Cha | 7 | K6 | K6.9+M1.0 | | 33.4 |
| RS Cha | 8 | A7 + A8 | eclipsing | | 34.9 |
| EN Cha | 9 | M4 | M4.4 + M4.7 | TO | 32.6 |
| EO Cha | 10 | M0 | | | 33.2 |
| EP Cha | 11 | K6 | | class II | 33.4 |
| EQ Cha | 12 | M3 | M3.2+M3.2: | | 32.7 |
| HD 75505 | 13 | A1 | | | 35.1 |
| ES Cha | 14 | M5 | | TO | 32.1 |
| ET Cha | 15 | M3 | | class II | 32.7 |

**Notes.** $^{(*)}$ Torres et al. (2008). $^{(**)}$ Sicilia-Aguilar et al. (2009), determined from Lyo et al. (2004). $^{(\dagger)}$ Sicilia-Aguilar et al. (2009). TO are transitional disk objects. $^{(\ddagger)}$ Luminosities determined from the spectral type, assuming an age of 6 Myr and the Siess et al. (2000)'s pre-main-sequence model.

the census of known cluster members grows up to twenty two (see Torres et al. 2008, for a recent review).

The proximity ($d \approx 97$ pc; Mamajek et al. 1999) and properties of $\eta$ Chamaleontis converts this cluster in an ideal target for pointed X-ray observations. In this paper, we present a detailed study of the X-ray properties of cluster members based on a new deep *XMM-Newton* observation. Details of this observation are presented in Section 2, together with the data reduction plan. In Section 3.1, we derive general coronal properties and treat to relate them with other stellar properties as binarity and the presence of accretion disks. X-ray variability (including flare-like variability) is studied in Section 3.2. In that section, we also investigate the relation between flare energies and different stellar parameters. Section 4 is dedicated to other possible members in the field-of-view of our observation. Notes on particular sources are given in Section 5. Finally, in Section 6 we briefly summarize the main results of this work.

## 2. X-ray observation and data reduction

Our *XMM-Newton* observation of the $\eta$ Chamaleontis cluster (id. 0605950101) was performed on a single exposure of 48.3 ks on June 2009. The EPIC was used in Full Frame mode with the Thick filter to reduce the contamination of the X-ray signal by visible and UV radiation. The effective exposure time of the observation was 46.4 ks in the EPIC-pn and 48.0 ks in the EPIC-mos. We performed a standard reduction using the version 9 of the specific *XMM-Newton* reduction package SAS. The observation was not affected by background flaring events and therefore, no time was lost by high X-ray variable background. For our study, we used a good-time-intervals events file, i.e cleaned for bad events and pixels and noise. The image shown in Fig. 1 was created by constructing a combined EPIC-pn+mos image using the task EMOSAIC of the SAS. EPIC images were first individually corrected for the quantum efficiency, filter transmission and mirror vignetting by dividing by the exposure maps obtained with the routine EEXMAP.

A modified version of the PWDetect code (Damiani et al. 1997) was used for the detection of sources in the 0.3–7.5 keV energy band. We chose the detection threshold $SNR = 5$, which corresponds to one possible spurious detection in each field, as obtained from our simulations of the background in *XMM-Newton*[1]. With this threshold, a total of 86 sources were detected in the combined EPIC-pn and mos image. A direct visual inspection allowed us to discard 7 multiple detections (sources detected more than once by the detection algorithm) plus two spurious detections in the detector borders. The complete list of source detections is given in Table A.1. For each source, we give its position, significance of the detection, observed count-rate and flux. This flux was determined by converting observed fluxes in photons cm$^{-2}$ s$^{-1}$ to erg cm$^{-2}$ s$^{-1}$ using the conversion factor $CF = 1.5 \pm 0.2 \times 10^{-9}$ erg ph$^{-1}$. This factor was determined from the spectral fitting of the known $\eta$ Chamaleontis members (see Section 3.1). Note that these fluxes are merely indicative. Most of the detected sources are Active Galactic Nuclei instead of stellar coronae. To check this fact, we suggest the reader to compare the fluxes determined for cluster members using the conversion factor (Table A.1) with the fluxes obtained from the spectral fitting (Table 2).

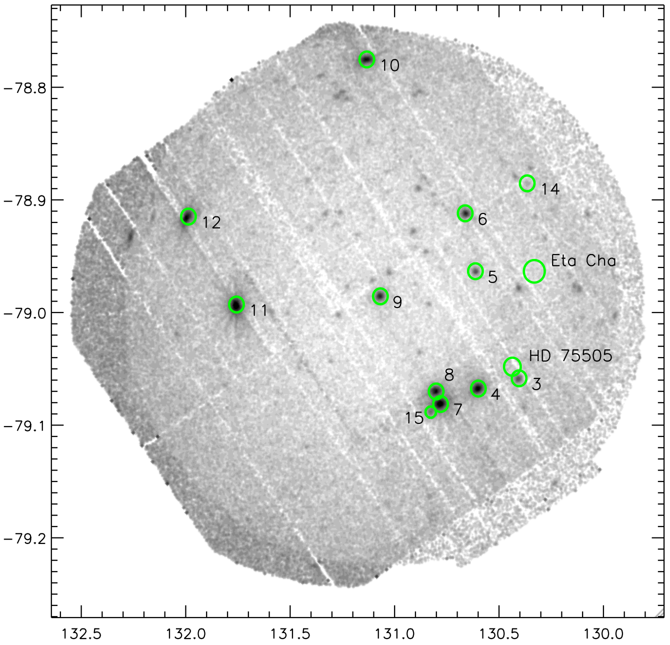

**Fig. 1.** EPIC-pn and mos mosaic of the $\eta$ Chamaleontis cluster. Known members of the cluster are marked with a circle and identified with its RECX number. The two members not detected in X-rays ($\eta$ Cha and HD 75505) are identified with their most common name instead of their RECX identification (RECX 2 and RECX 13, respectively).

The value used by us as detection threshold corresponds to a source count-rate limit of completeness $CR = 5.5 \pm 1.5 \times 10^{-4}$ s$^{-1}$ in the EPIC energy band. Assuming a typical corona with $kT \sim 0.5 - 1$ keV, this count-rate corresponds to a flux $f_{\rm X} \sim 1{-}3 \times 10^{-15}$ erg cm$^{-2}$ s$^{-1}$, or $L_{\rm X} \sim 2 \times 10^{27}$ erg s$^{-1}$ at a distance of 100 pc (an upper limit to the distance of cluster members). This assures us that all the cluster members emitting in X-rays have been detected. Compared to observations of other clusters and star-forming regions, our observation is one order of magnitude deeper in X-ray luminosities.

In Fig. 1 we mark with a circle the position of the known cluster members in the field of view of our observation. Note that two of them were not detected: the B star $\eta$ Cha and the A star HD 75505 (see Section 5 for details).

---

[1] We acknowledge Dr. I. Pillitteri for his help with the *XMM-Newton* background simulations

## 3. General X-ray properties of $\eta$ Chamaleontis members

### 3.1. General properties

The fourteen known cluster members in the EPIC field of view include three early-type stars: $\eta$ Cha (B8 V), HD 75505 (A0 V), and RS Cha (A7 V) and 11 Li-rich, $H_\alpha$ emission-line late-type (K6–M5) stars. The first X–ray characterization of this region was performed by Mamajek et al. (1999) based on pointed *ROSAT*-HRI [0.1-2.4 keV] broadband observations (see Section 1 for details). Unfortunately, those observations did not allow the authors to perform a complete spectral characterization of the detected sources, due to the limited spectral response of the HRI (see Mamajek et al. 2000). With the *XMM-Newton* [0.3-10 keV] observation, we are able to give parameters of the hot plasma by fitting plasma models to the X-ray spectrum of each star.

It is important to note here that, for our study, we assume that all the X-ray emission comes from the (hot) coronal plasma. This is basically correct for non-accreting stars. However, it has been demonstrated that accretion shocks generate dense, relatively hot plasma that emits in very soft X-rays (e.g. Sacco et al. 2008; Brickhouse et al. 2010). Its contribution to the overall stellar X-ray emission is negligible in medium and hard X-rays ($kT \geq 0.5$ keV). But, when the accretion rate is high (of the order of $\sim 10^{-10}$ $M_\odot$ yr$^{-1}$), the X-ray luminosity from the shocked plasma is of the same order of magnitude than the typical X-ray luminosity of a T Tauri star (see Sacco et al. 2008). Of the four accreting stars in our sample, only one (RECX 15) shows a high accretion rate (e.g. Sicilia-Aguilar et al. 2009). Nevertheless, it is highly absorbed in soft X-rays (see Table 2 and discussion below). Thus, the contribution of X-rays produced by the accretion to its spectrum is presumably very low, although high resolution observations are needed to investigate this fact.

The EPIC spectra – integrated for the whole exposure – were analyzed using a 2T-temperature model. In some cases, a third temperature was added to obtain a robust fit at hard (i.e. above 2 keV) X-ray energies. We note here that the stars for which a 3-T model was used underwent flare-like events during the exposure (see Section 3.2). For them, we performed a more detailed study separating the quiescent from the flare state. The results of this study are shown in Table 4 and in Section 3.2. For the fit, we used the Astrophysical Plasma Emission Code (APEC, Smith et al. 2001a) which is included in the XSPEC spectral fitting package (Arnaud 1996, 2004). APEC is a routine that generates spectral models for hot (optically thin) plasmas using the atomic data contained in the Astrophysical Plasma Emission Database (APED, Smith et al. 2001b). We added a multiplicative interstellar absorption model in XSPEC – in particular the one described in Morrison & McCammon (1983) – to account for possible absorption due to interstellar and/or circumstellar material (for a more detailed description of the method we refer the reader to López-Santiago & Caballero 2008).

Best-fit parameters for the chosen models were found by $\chi^2$ minimization and are shown in Fig. A.1. A word of caution is necessary here: the resulting fits as given below are merely formal and indicative. A 2-T model fitting to an observed coronal spectrum does not mean that we have to deal with two different plasmas at two different temperatures. In general, the coronal plasma exhibits a temperature gradient that cannot be studied using low-resolution X-ray spectra (although see Robrade & Schmitt 2005). Nevertheless, it has been shown that the dual-temperature nature of the fits may represent an intrinsic property of the coronal spectra of moderately active late-K and M stars (Schmitt et al. 1990; Briggs & Pye 2003; López-Santiago et al. 2007). In this scenario, the third (higher) temperature required to fit the hard tail of the X-ray spectrum is though to be present only during flare-like events. In most cases, a successful 1-T model fitting is a mere reflection of a lack of information due to the low statistics (i.e. count-rate) of many sources.

In Table 2 we give details on the best-fit parameters for each star. As a goodness-of-fit test, we give the reduced $\chi^2$ and degrees of freedom (d.o.f.) used for the fit. Unabsorbed fluxes in the energy band 0.3–8.0 keV are also given. Finally, the X-ray luminosities listed in the table were determined using the same distance for all the stars ($d = 97$ pc). It is noticeable that our luminosities are 0.2–0.3 dex smaller than those determined by Mamajek et al. (2000) in a smaller energy range, except for EN Cha (RECX 9) and EP Cha (RECX 11) that underwent long duration flares during our exposure (see Section 3.2 and Fig. A.2). Nevertheless, it must be said that the authors could not perform model fitting to their data because of the poor spectral response of the *ROSAT*-HRI. Mamajek et al. (2000) then used a conversion factor to derive X-ray fluxes from the observed count-rates. Besides, they could not correct the observed fluxes for absorption. Taking all these factors into account, their estimations of the X-ray luminosities of the $\eta$ Chamaleontis members were quite reasonable.

The results presented in Table 2 about the coronal temperature should be interpreted with caution, since different effects are contributing to the X-ray spectra. On average, the corona of the stars showing no flares during our observation are parametrized by a 2T-model with temperatures $kT_1 \approx 0.30$ keV and $kT_2 \approx 0.95$ keV. For stars that underwent a flare during the exposure, a third (hotter) component needs to be added to the model. For the two stars with lower count-rates (i.e. lower statistics), in which a 1T-model was used, the temperature obtained from the fit represents a mean value between $kT_1$ and $kT_2$, weighted by the emission measure. We refer the reader to López-Santiago et al. (2007) and Caballero et al. (2010) for a more detailed discussion on this issue. These results suggest that the X-ray spectrum of these stars during their quiescent state can be parametrized by a plasma model typical of both main- and pre-main-sequence stars. Only the star EN Cha (RECX 9) deviates from this trend ($kT_1 \approx 0.77$ keV, $kT_2 \approx 2.22$ keV). The reason is likely that its X-ray spectrum is highly absorbed (at longer wavelengths) due to the presence of a circumstellar disk (Sicilia-Aguilar et al. 2009), rather than it is caused by high X-ray emission produced during a flare-like event. Note that the star underwent a flare before the beginning of the exposure while we observed only the decay phase (see Fig. A.2), were the plasma is rapidly cooling. The spectral analysis of the known cluster members gave low mean column densities, with mean $N_\mathrm{H} = 4.6 \times 10^{20}$ cm$^{-2}$, with typical deviation $\sigma = 8.5 \times 10^{20}$ cm$^{-2}$. The observed dispersion is due to the high $N_\mathrm{H}$ values found for the sources RECX 9 and 15. Both are well-known CTTS (e.g. Sicilia-Aguilar et al. 2009).

To investigate possible correlations between average X-ray luminosity and any stellar parameter, such as binarity, mass, or the presence of accretion disks, we used data from the literature (see Table 1). In Fig 2 we plot different symbols for each object type (as classified by Sicilia-Aguilar et al. 2009): classical T Tauris (CTTSs, circles), transitional disk objects (TO, triangles), and weak-line T Tauris (WTTSs, squares). Filled symbols are

**Table 2.** Spectral parameters of known members

| RECX | $N_H$ ($\times 10^{21}$ cm$^{-2}$) | $kT_1$ (keV) | $kT_2$ (keV) | $kT_3$ (keV) | $EM_1/EM_2$ | $EM_1/EM_3$ | $Z$ ($Z_\odot$) | $\chi^2$ (d.o.f.) | Unabsorbed $f_X$ ($\times 10^{-13}$ erg cm$^{-2}$ s$^{-1}$) | log $L_X$ (erg s$^{-1}$) | log $L_X$** (erg s$^{-1}$) |
|---|---|---|---|---|---|---|---|---|---|---|---|
| 3 | $0.00^{+0.31}_{-0.00}$ | $0.63^{+0.04}_{-0.04}$ | ... | ... | ... | ... | $0.08^{+0.02}_{-0.02}$ | 1.12 (88) | $0.65^{+0.06}_{-0.10}$ | 28.9 | 29.2 |
| 4 | $0.44^{+0.12}_{-0.11}$ | $0.28^{+0.02}_{-0.01}$ | $0.96^{+0.04}_{-0.03}$ | ... | 0.92 | ... | $0.12^{+0.02}_{-0.01}$ | 1.29 (402) | $6.61^{0.71}_{2.97}$ | 29.9 | 30.2 |
| 5 | $0.00^{+0.25}_{-0.00}$ | $0.27^{+0.07}_{-0.06}$ | $0.74^{+0.18}_{-0.09}$ | ... | 1.30 | ... | $0.10^{+0.06}_{-0.03}$ | 0.96 (162) | $0.56^{+0.04}_{-0.12}$ | 28.8 | 29.1 |
| 6 | $0.23^{+0.22}_{-0.19}$ | $0.33^{+0.04}_{-0.03}$ | $0.95^{+0.05}_{-0.06}$ | ... | 0.88 | ... | $0.13^{+0.04}_{-0.03}$ | 0.93 (347) | $2.47^{+0.35}_{-0.20}$ | 29.4 | 29.6 |
| 7 | $0.03^{+0.13}_{-0.03}$ | $0.33^{+0.01}_{-0.01}$ | $0.94^{+0.05}_{-0.04}$ | $2.08^{+1.42}_{-0.36}$ | 0.75 | 2.21 | $0.19^{+0.03}_{-0.04}$ | 1.03 (491) | $10.50^{+0.78}_{-0.50}$ | 30.1 | 30.4 |
| 8 | $0.00^{+0.10}_{-0.00}$ | $0.26^{+0.06}_{-0.03}$ | $0.76^{+0.08}_{-0.06}$ | $1.54^{+0.14}_{-0.13}$ | 0.87 | 0.61 | $0.26^{+0.05}_{-0.05}$ | 1.28 (353) | $4.05^{+0.39}_{-0.31}$ | 29.7 | 29.9 |
| 9 | $2.89^{+0.24}_{-0.29}$ | $0.77^{+0.02}_{-0.04}$ | $2.22^{+0.18}_{-0.18}$ | ... | 0.47 | ... | $0.30^{+0.13}_{-0.06}$ | 1.12 (518) | $2.95^{+0.21}_{-0.38}$ | 29.5 | 28.5 |
| 10 | $0.04^{+0.19}_{-0.04}$ | $0.40^{+0.09}_{-0.04}$ | $0.98^{+0.05}_{-0.06}$ | ... | 0.72 | ... | $0.15^{+0.04}_{-0.04}$ | 0.92 (300) | $4.07^{+0.39}_{-0.31}$ | 29.7 | 30.0 |
| 11 | $0.06^{+0.01}_{-0.01}$ | $0.25^{+0.02}_{-0.01}$ | $0.95^{+0.04}_{-0.04}$ | $2.52^{+0.45}_{-0.27}$ | 0.90 | 1.20 | $0.21^{+0.10}_{-0.05}$ | 1.20 (805) | $27.93^{+1.37}_{-2.83}$ | 30.5 | 30.2 |
| 12 | $0.11^{+0.20}_{-0.11}$ | $0.28^{+0.02}_{-0.02}$ | $1.00^{+0.03}_{-0.03}$ | $2.90^{+3.51}_{-0.99}$ | 0.73 | 2.45 | $0.20^{+0.10}_{-0.09}$ | ... | $10.90^{+1.10}_{-0.58}$ | 30.1 | 30.2 |
| 14* | ... | ... | ... | ... | ... | ... | ... | ... | ... | ... | ... |
| 15 | $1.27^{+0.47}_{-0.52}$ | $0.80^{+0.18}_{-0.09}$ | ... | ... | ... | ... | $0.04^{+0.02}_{-0.02}$ | 1.05 (64) | $0.31^{+0.07}_{-0.24}$ | 28.8 | ... |

**Notes.** (*) The background subtracted spectrum of RECX 14 has only 67 counts. We failed any attempt of fitting a plasma model. (**) X-ray luminosities determined by Mamajek et al. (2000) in the 0.1–2.0 *ROSAT* energy band.

stars with flare events during our observations. For these stars, we plot also the X-ray luminosity in the pseudo-quiescent state (see Section 3.2.1). Large circles mark binary stars. The upper-limit symbol used for RECX 11 denotes that its quiescent-state X-ray emission is probably lower than that determined from our observations. Note that, for our study, we assumed the emission in the time-period $20 < t < 30$ ks to be representative of the quiescent state of this star but this period is between two flare events (see Fig. A.2). No particular differences between the X-ray luminosity of binary and single stars or stars with and without an accretion disk is detected, although the sample is not large enough to extract any robust conclusion from this result. The typical trend of decreasing X-ray luminosity with decreasing mass (Preibisch et al. 2005) is observed. Nevertheless, the stars that underwent a flare during our observations have higher luminosities than stars with no flares, even when the contribution of the flare is subtracted. Note that EQ Cha (RECX 12) very probably underwent a flare during the observations. A 3T-model with k$T_3$ = 2.90 keV was necessary for the fit (see Table 2). This difference in the X-ray luminosities for stars with similar spectral types may be explained by an enhancement of the X-ray emission (quiescent) level before the flares occur. This explanation should be interpreted with caution, since the statistic in terms of number of stars is very poor.

### 3.2. X-ray variability

X-ray variability in time scale of days was reported by Mamajek et al. (2000) for seven cluster members. The authors attributed this variability to flare-like events superposed on moderately variable emission, but the poor signal of those observations prevented them to perform a quantitative analysis. In general, moderate variations in scale of a few days are probably owed to rotational modulation (Marino et al. 2003). Examples of it are shown in Caballero et al. (2009) for the $\sigma$ Orionis cluster and Flaccomio et al. (2005) for Orion. Flare-like events are usually short in time (from a few minutes to a few hours) and imply a large release of energy. In young stars and particularly in T Tauri stars, they have been observed in a large variety of shapes (e.g. Favata et al. 2005; Franciosini et al. 2007; López-Santiago et al. 2010). The *Chandra* and, specially, the *XMM-Newton* missions due to its large collector area, are powerful to detect flaring events in stars. In this sense, our observation is suitable to detect short-time (< 30 minutes) and medium-time (several hours) variations.

**Table 3.** Characteristics of the variations of the $\eta$ Chamaleontis members.

| Source | RECX | Ext. radius (arcsec) | Time bin (s) | Type | Factor | Flare dur. (ks) |
|---|---|---|---|---|---|---|
| EH Cha | 3 | 15 | 1500 | | | |
| EI Cha | 4 | 15 | 900 | Flare | 2.7 | >10 |
| EK Cha | 5 | 15 | 1200 | | | |
| EL Cha | 6 | 15 | 900 | Flare | 2.6 | ~4 |
| EM Cha | 7 | 15 | 900 | Variable | | |
| RS Cha | 8 | 10 | 1000 | Flare | 1.8 | ~20 |
| EN Cha | 9 | 15 | 900 | Flare | >7.3 | >40 |
| EO Cha | 10 | 23 | 900 | Variable | | |
| EP Cha | 11 | 32 | 900 | Flare | 1.4/1.7 | ~18/16 |
| EQ Cha | 12 | 32 | 1200 | Flare? | | |
| ES Cha | 14 | 8 | 1200 | | | |
| ET Cha | 15 | 12 | 1800 | Flare? | | |

We extracted light curves from the EPIC-pn for the cluster members revealed in our observation, except for RECX 12, for which we used EPIC-mos since it was located in a gap between chips in the EPIC-pn. We chose a specific extraction radius for each source, depending on the position of the source at the detector, to avoid the lost of counts due to the degradation of the PSF towards the borders of the EPIC. A background region was chosen close to the source, in the same chip but far from other sources, and then subtracted from the source light curve. A different time binning was also used for each source depending on the source count-rate. The resultant background-subtracted light curves are shown in Fig. A.2. In Table 3, we give details on the parameters for the extraction of the light curves (extraction radius and time binning), the type of variability detected and the count-rate increase factor during the flare in those stars in which a flare was clearly detected. We classified the type of variability as *flare*, when flare-like events where observed, or simply *variable*, for other types of variability. RECX 15 (ET Cha) is revealed above the background only in a small fraction of the exposure, around 30 ks from the beginning of the observation. We suspect this star underwent a flare an that its quiescent emission is below the detection limit of this observation.

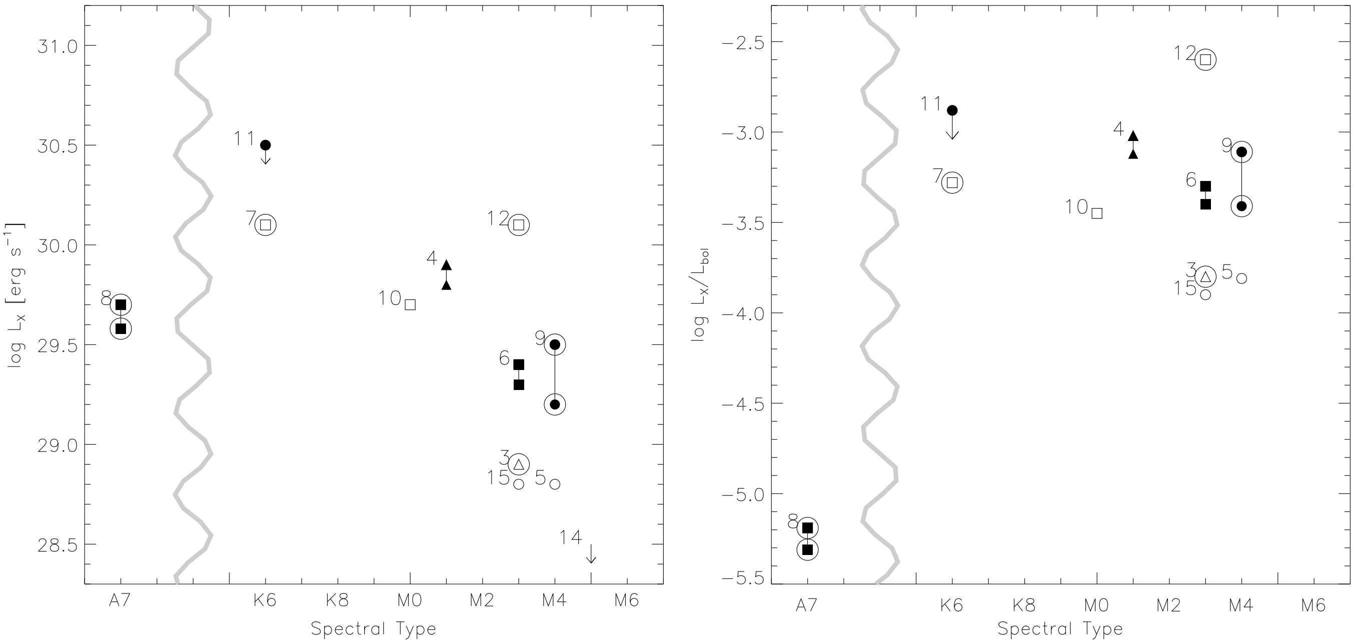

**Fig. 2.** X-ray luminosities of known members of $\eta$ Chamaleontis in the energy band 0.3–8.0 keV. Circles are known classical T Tauri stars, triangles are transitional objects and squares are stars with no signatures of accretion disks. Filled symbols mark stars that underwent a flare during our observation. Binary systems are marked with a large circle. Note that RECX 12 was observed, probably, in flare state during the exposure but was not clearly detected in its light curve due to its low count-rate (see Section 3.1).

### 3.2.1. Flares

During the exposure time, five stars showed clear flare activity (see Fig. A.2). Flares detected in our observation are not very intense in terms of count-rate enhancement (see Table 3). Count-rate increase factors of approximately 2 – 3 were detected, except for EN Cha (RECX 9). These values are similar to those observed in the less energetic flares detected in Taurus (Franciosini et al. 2007) and in M field stars (Robrade & Schmitt 2005; López-Santiago et al. 2007; Crespo-Chacón et al. 2007). In this sense, flares detected in members of $\eta$ Chamaleontis are similar to those observed in other M-type stars.

We studied plasma parameters during the flares. In Table 4 we give the results of the fits of hot plasma models to the X-ray spectrum of the stars during the flare and the *quiescent* state for each star (assumed to be the characteristic level shown by the star previously to the flare, except for RECX 9, for which we used the last 6 ks of observation). As in the previous subsection, for the fit we used the XSPEC spectral fitting package with the APED and the WABS model (see Section 3.1). A $1T$–model was used for the quiescent state, except for RECX 4 and RECX 11, for which it was necessary to add a second thermal component to fit the spectrum. Note that they are the sources with the higher mean count-rates. The goodness of the fit is given in the table as the reduced $\chi^2$. For the flares, the fit was done after subtracting the quiescent spectrum. An absorbed $1T$–model was then used, maintaining the same values of $N_{\rm H}$ and $Z$ than for the quiescent state. Note that temperatures obtained here are mean values, since we are integrating the entire event. The X-ray luminosities for the quiescent and the flare given in Table 4 are corrected for absorption. A mean distance of 97 pc was used to transform fluxes to luminosities for each star. $L_{\rm X}^{\rm fl}$ and $\log E_{\rm X}^{\rm fl}$ are, respectively, the X-ray luminosity and liberated energy during the flare event. Fluxes, luminosities and energies were determined in the [0.3–8.0] energy band. Note that our results for the flare parameters are relative to the pseudo-quiescent level chosen for the analysis. In particular, RECX 9 is observed during a flare decay phase and we used the last 8 ks of exposure as its quiescent level. In general, the values obtained here for the flare energies are consistent with those found for members of Taurus (see below).

Flare energies determined for our stars are typical of pre-main-sequence M stars. There seems to be none correlation with spectral-type, binarity or the presence of disks. The energy liberated during the flare in RECX 6 (the only star with no signs of disk among this group of stars showing flares) is one order of magnitude lower than for the others. However, this result is not determining because of the small sample we are using. We have compared our results with those obtained for the Taurus region by Stelzer et al. (2007). In Fig. 3 we plot flare energies observed for the stars in our sample (triangles) compared with those in the *XMM-Newton* Extended Survey of the Taurus molecular cloud (XEST; plusses). Filled triangles and large symbols are used to mark stars with disks in our sample and the XEST one, respectively. Except for RECX 6 (with a flare energy $\log E_{\rm flare}$ [erg] = 32.6), the stars in our sample show flare energies similar to those in the XEST with the same spectral type. No difference between stars with and without disk is observed. The stars marked with a circle in Fig. 3 are classified as classical T Tauri in Güdel et al. (2007) and the stars marked with a square are embedded stars.

### 3.2.2. X-ray emission modulation

Six stars in our sample showed some kind of modulation in their light curves during the observations. These stars have RECX numbers 6, 7, 10, 11, 12, and 15. In RECX 6 and RECX 11, the observed variations may be related to the decay of precedent flares. In particular, RECX 11 seems to show two flares during

**Table 4.** Best fit values of the spectral model parameters for the quiescent and the flare. Errors are 90% confidence level. X-ray luminosities and flare energies are unabsorbed values. We assumed a distance of 97 pc for all the stars. Fluxes, luminosities and energies were determined in the [0.3–8.0] energy band.

| | Quiescent | | | | | | | Flare | | | | |
|---|---|---|---|---|---|---|---|---|---|---|---|---|
| Source RECX | $N_{\rm H}$ ($\times 10^{21}$ cm$^{-2}$) | $Z$ ($Z_\odot$) | $kT_1$ (keV) | $kT_2$ (keV) | $EM_1/EM_2$ | $\chi^2_{\rm q}$ | $\log L_{\rm X}^{\rm q}$ (erg s$^{-1}$) | $kT_{\rm fl}$ (keV) | $EM_1/EM_{\rm fl}$ | $\chi^2_{\rm fl}$ | $\log L_{\rm X}^{\rm fl}$ (erg s$^{-1}$) | $\log E_{\rm X}^{\rm fl}$ (erg) |
| 4 | $0.3^{+1.4}_{-0.8}$ | $0.13^{+0.03}_{-0.02}$ | $0.29^{+0.02}_{-0.02}$ | $0.91^{+0.04}_{-0.04}$ | 0.99 | 1.10 | 29.8 | $2.27^{+0.44}_{-0.48}$ | 0.77 | 1.07 | 29.9 | >33.6 |
| 6 | $0.0^{+0.2}_{-0.0}$ | $0.08^{+0.02}_{-0.03}$ | $0.73^{+0.04}_{-0.06}$ | ... | ... | 0.84 | 29.3 | $3.17^{+24.8}_{-1.83}$ | 5.54 | 0.81 | 28.8 | 32.6 |
| 8 | $0.3^{+0.4}_{-0.1}$ | $0.05^{+0.03}_{-0.02}$ | $0.74^{+0.08}_{-0.11}$ | ... | ... | 1.09 | 29.7 | $1.05^{+0.33}_{-0.32}$ | 3.94 | 0.75 | 29.2 | 33.6 |
| 9 | $1.6^{+0.4}_{-0.7}$ | $0.13^{+0.13}_{-0.02}$ | $1.24^{+0.37}_{-0.21}$ | ... | ... | 0.70 | 29.2 | $1.54^{+0.35}_{-0.37}$ | 0.32 | 1.08 | 29.8 | >34.4 |
| 11 (1st flare) | $1.0^{+0.2}_{-0.3}$ | $0.12^{+0.04}_{-0.03}$ | $0.26^{+0.02}_{-0.01}$ | $1.21^{+0.06}_{-0.06}$ | 1.70 | 1.10 | 30.5 | $2.12^{+1.08}_{-0.58}$ | 6.09 | 1.15 | 29.8 | 33.8 |
| 11 (2nd flare) | $1.0^{+0.2}_{-0.3}$ | $0.12^{+0.04}_{-0.03}$ | $0.26^{+0.02}_{-0.01}$ | $1.21^{+0.06}_{-0.06}$ | 1.70 | 1.10 | 30.5 | $1.49^{+0.55}_{-0.35}$ | 3.76 | 1.11 | 30.0 | 34.0 |

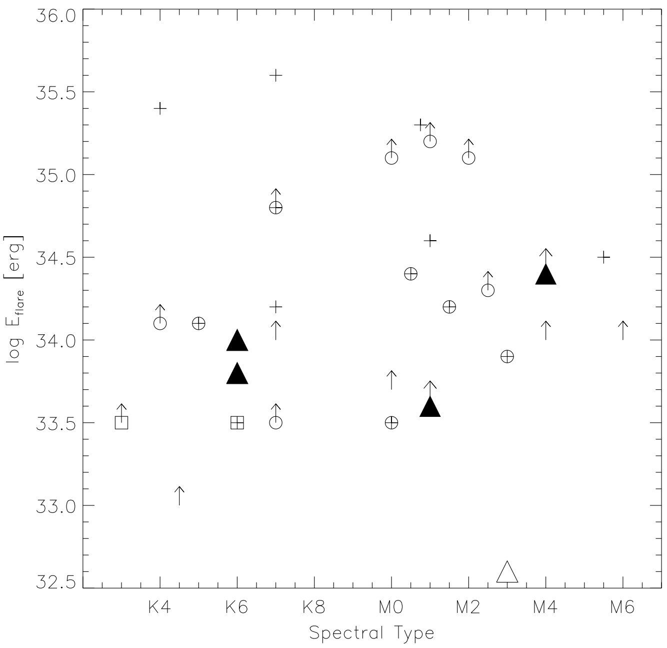

**Fig. 3.** Energy liberated during the flare in the [0.3–8.0] energy band for the stars in our sample (large triangles) and the stars of the XEST (plusses; Stelzer et al. 2007). Upward arrows denote lower limits. Filled triangles are stars with a disk in $\eta$ Chamaleontis. Stars classified as classical T Tauri in Güdel et al. (2007) are marked with a large symbol (square or circle).

the observing period. In the remaining stars, the variations may be related to rotational modulation.

The particular cases of RECX 7 and RECX 10 are interesting since they show a decrease in count-rate during a short period of time (~3 and 1.5 hours respectively). This decrease could be related to an occultation of the corona by a companion. Of them, RECX 7 is known to be a double-line binary (Mamajek et al. 1999) with a period of 2.6 days (Lyo et al. 2003). However, RECX 10 has none known companion (Guenther et al. 2007).

## 4. Candidate cluster members in the field of view

Because of the low flux limit of our observation, we expected to detect all the cluster members emitting in X-rays in the EPIC field of view (see Section 2). Based on optical photometry, Mamajek et al. (2000) selected 50 candidates in the cluster core region. Later, Lawson et al. (2002) confirmed two low-mass stars inside the *ROSAT* field of view to be members of $\eta$ Chamaleontis using optical spectroscopy. They were not detected during the *ROSAT* observations. These two stars have RECX numbers 14 and 15 and have been both detected in our observation (see Section 2 and Table A.1). The searching radius for candidates has been increasing since then up to 5.5 deg (Luhman 2004; Lyo et al. 2004; Song et al. 2004; Lyo et al. 2006; Murphy et al. 2010). Six new members and 3 possible members have been identified at distances of between 1 and 6 deg from the cluster core. Most of these surveys were centered on finding very low mass stars and brown dwarfs cluster members (e.g. Luhman 2004; Lyo et al. 2006; Murphy et al. 2010).

We searched for intermediate-mass (late-F and G type stars) members of the $\eta$ Chamaleontis cluster that, eventually, would had gone unnoticed in low-mass and brown dwarfs surveys. Those stars should emit in X-rays with fluxes above our detection limit ($f_{\rm X} \sim 1 - 3 \times 10^{-15}$ erg cm$^{-2}$ s$^{-1}$; see Section 2). We first cross-correlated our X-ray sample with the 2MASS database (Skrutskie et al. 2006). A searching radius of 4 arcsec was used to prevent *false* positives in the identification. Della Ceca et al. (2004) estimated a positional error of the X-ray sources of the XMM-Newton Bright Serendipitous Survey of 6 arcsec. However, the mean distance between known members cluster and its X-ray counterpart in our observation is ~ 1.8 arcsec with a maximum separation of 2.8 arcsec for RECX 11. A searching radius of 4 arcmin is a conservative value.

The results of cross-correlating our X-ray sample and the 2MASS database are shown in Fig. 4. Small dots in the figure are 2MASS sources in the field of view of EPIC. Filled circles are the fourteen known cluster members in the same field of view. The twelve members detected in this observation are marked with a larger circle. Open circles are other X-ray sources in the field with a 2MASS counterpart. ZAMS and 8 Myr isochrone are also plotted. From these figures, only one of these other X-ray sources could be classified as possible member of the cluster. The star (2MASS J08483486-7853513) has near-infrared colors of an M4/6 dwarf, which would correspond to a mass of 0.10–0.13 $M_\odot$ for a cluster member. However, Lawson et al. (2002) already studied this star and found that it is likely a high-proper-motion dM5e foreground star at a distance of ~ 50 pc. The other three sources are background stars (see Fig. 4 and Table 5). Note that there is only one star in the field that could fulfill the requirement to be an intermediate-mass (FG-type star) cluster member in terms of near-infrared colors. This star is HD 76144. Nevertheless, the Hipparcos catalog gives a distance $d = 140$ pc, quite larger than the value estimated for the cluster members. The star is neither detected in the *XMM-Newton* observation with our detection procedure (see Section 2). Therefore, we neglected also this star as a member of $\eta$ Chamaleontis.

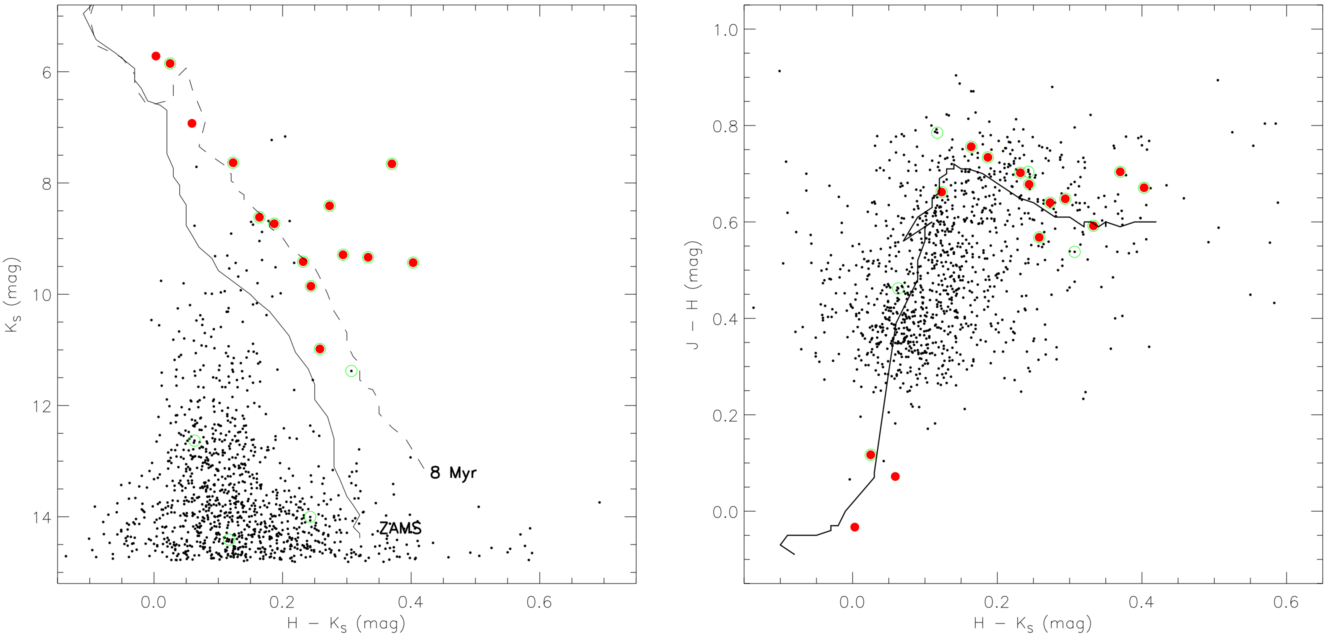

**Fig. 4.** 2MASS color-magnitude and color-color diagrams of the X-ray sources detected in the XMM-Newton image, plus $\eta$ Cha. Filled circles are the known cluster members in the EPIC field of view. Those members detected in our observation are marked with a larger circle. Open circles are X-ray sources in our list of detections. Small dots are 2MASS sources in the field of view. ZAMS and 8 Myr isochrones are a combination of pre-main sequence models by Siess et al. (2000), for intermediate-mass stars and Baraffe et al. (1998), for low-mass stars. In the color-color diagram, we plot only the 8 Myr isochrone.

**Table 5.** Other X-ray sources in the field with 2MASS counterpart non-members of $\eta$ Chamaleontis.

| 2MASS | $J$ (mag) | $H$ (mag) | $K_S$ (mag) | Note |
|---|---|---|---|---|
| J08394669-7900026 | 17.21 ± 0.22 | 16.42 ± 0.22 | 15.56 ± 0.23 | Galaxy |
| J08431595-7853422 | 14.95 ± 0.03 | 14.25 ± 0.04 | 14.00 ± 0.06 | M-type |
| J08440921-7906156 | 15.31 ± 0.05 | 14.53 ± 0.06 | 14.41 ± 0.07 | K-M giant |
| J08451844-7854426 | 13.16 ± 0.03 | 12.69 ± 0.02 | 12.63 ± 0.03 | K-type |
| J08483486-7853513 | 12.22 ± 0.02 | 11.69 ± 0.03 | 11.40 ± 0.02 | dM5e$^{*}$ |

**Notes.** $^{(*)}$ Lawson et al. (2002) rejected this star as a cluster member and gave spectral type M5 with emission. Luhman (2004) confirmed this result later.

## 5. Notes on individual stars

### 5.1. $\eta$ Cha (RECX 2)

This star is the most massive cluster member (spectral type B8). It was detected by Mamajek et al. (1999) in a *ROSAT*-HRI observation. From the observed X-ray flux, they inferred an X-ray luminosity $\log L_{\rm X}[{\rm erg\,cm^{-2}\,s^{-1}}] = 28.8$ in the HRI energy band. Mamajek et al. (2000) later suggested that $\eta$ Cha is likely a binary star, based on the observed variations in its radial velocity (Buscombe & Morris 1961). Therefore, they argued that the X-ray emission is likely to be produced in a low-mass secondary, for which Lyo et al. (2004) estimates a mass of $0.5\,M_\odot$ using $L_{\rm X} - M$ relationships.

$\eta$ Cha was not detected in our *XMM-Newton* observation. At our detection flux limit $f_{\rm X} \sim 1 - 3 \times 10^{-15}$ erg cm$^{-2}$ s$^{-1}$ in the energy band [0.3-8.0] keV – which is traduced in a luminosity $L_{\rm X} \sim 2 \times 10^{27}$ erg s$^{-1}$ at a distance of 100 pc – any low-mass companion should have been detected (although see Section 3.2, where we suggest that ET Cha has a quiescent X-ray emission lower than the detection limit). The lack of X-ray emission from this star during the entire exposure is not simply explained in terms of variability. A possible scenario would be one in which the primary (non-emitting) star would eclipse the X-ray emitter for long periods of time. Nevertheless, the fact that the X-ray emission would had gone unnoticed during this observation should not be discarded. Note that ES Cha (RECX 14), the member with the lowest mass in the field of view, was observed at the detection limit. A lower mass star (spectral type latter than M6) or even a brown dwarf may be part of this system. Any of these scenarios should be checked through a robust determination of the system orbital parameters.

### 5.2. RS Cha (RECX 8)

RS Cha is a well-known Herbig Ae double-lined eclipsing binary with an orbital period $P_{\rm orb} = 1.67$ days, located in the instability strip (Marconi & Palla 1998; Alecian et al. 2005). The pulsating nature of both stars in the system was confirmed by Böhm et al. (2009).

The X-ray emission detected with *ROSAT* by Mamajek et al. (1999) has been suggested to come from a tertiary companion (Mamajek et al. 2000; Lyo et al. 2004). However, Alecian et al. (2005) found evidences that the time for the first conjunction of this system changes with time very rapidly, what is not expected for the presence of a third body in the system. Instead, the soft X-ray emission may come from the A-type stars themselves, especially if they have disturbed atmospheres (Gómez de Castro 2009). But it has been shown that X-ray spectral properties of Herbig Ae/Be stars are similar to those observed in late-type stellar companions to other Herbig Ae/Be stars (e.g. Stelzer et al. 2006, 2009). In fact, the X-ray luminosity of RS Cha is similar to that observed for the early-type M members of the cluster (see Fig. 2).

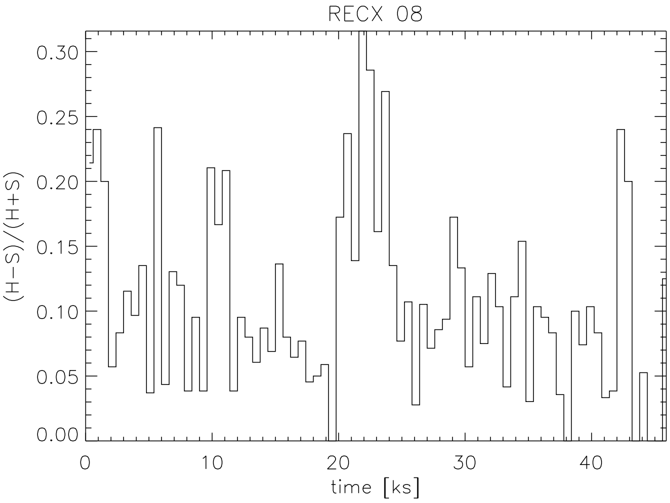

**Fig. 5.** Evolution of the hardness-ratio of RS Cha with time. The soft ($S$) and hard ($H$) energy bands are defined in the ranges [0.3-0.8] and [2.0-7.5] keV, respectively. Each bin is 10 minutes long.

In the *XMM-Newton* observation, RS Cha underwent a flare. This fact is confirmed by the temporal evolution of the spectrum hardness-ratio (Fig. 5). Besides, from the ephemeris for the primary minimum given by Clausen & Nordstrom (1980) and the linear variation of this relation with time observed by Alecian et al. (2005), we estimate the primary eclipse finished $\sim$ 2.3 hours after the beginning of the exposure, more than three hours before the flare occurred. Therefore, the shape of the light curve cannot be produced by an occultation of the X-ray emitter.

The flare temperature determined from the X-ray spectrum is quite low and the amount of material involved in the flare event is not very large compared with the quiescent (see Table 4). In this sense, the event detected in RS Cha is not very different from those observed in late-type cluster members as EP Cha (RECX 11).

### *5.3. EM Cha and EO Cha (RECX 7 and RECX 10)*

During the observation, both stars presented a decrease of their count-rate by a factor of $\sim$ 1.5 during 3 and 1.5 hours, respectively, in a way that resembles the occultation of part of the stellar corona by a companion (see Fig. A.2). EM Cha is known to be a binary star with a mass ratio of approximately 2.3:1 (Lyo et al. 2004). Following the results of Section 3.1, the low-mass companion may have an X-ray luminosity of 0.5–1 orders of magnitude lower than the primary (see Fig. 2). The occultation of part of the corona of the primary star by the secondary would produce a decrease of the observed total flux (i.e. of the observed count-rate). EO Cha, however, shows none sign of binarity (Guenther et al. 2007; Lyo et al. 2004). Therefore, the eclipse scenario does not seem probable for EO Cha.

The observed light curves may also be explained, in both cases, by the occultation of an active region behind the visible stellar hemisphere due to stellar rotation. In fact, the count-rate of EO Cha increased during approximately 2.5 hours before the rapid decrease during 1.5 hours at the middle of the exposure. This fact may be interpreted as the occultation of an active region by the star's disk. Nevertheless, with the available data, none of these two scenarios can be discarded.

### *5.4. EN Cha (RECX 9)*

EN Cha is a classical T Tauri, binary system (Köhler & Petr-Gotzens 2002; Sicilia-Aguilar et al. 2009) formed by two nearly identical M-type stars (Mamajek et al. 2000; Lyo et al. 2004). During the *ROSAT* observation, this star was marginally detected above the background level, with an X-ray luminosity $\log L_{\rm X}[\rm erg\,cm^{-2}\,s^{-1}] = 28.5$ (Mamajek et al. 2000). During the *XMM-Newton* observation, the star showed a luminosity one order of magnitude higher than during the *ROSAT* observation.

From the light curve and coronal parameters obtained from the plasma model fitting (Fig. A.2 and Table 3), it seems clear that EN Cha underwent a flare during the *XMM-Newton* observation.

## 6. Summary and conclusions

In this paper we presented a detailed study of the X-ray emission properties of the $\eta$ Chamaleontis cluster members, based on a deep *XMM-Newton* observation toward the cluster core. This study is complete in terms of cluster members. We detected all the (X-ray emitter) members of $\eta$ Chamaleontis down to the substellar mass limit. We determined X-ray luminosities, coronal temperatures, abundances and column densities from hot plasma model-fitting. We also studied the variability of the sources.

The comparison between the X-ray luminosities derived in this work and those obtained by Mamajek et al. (2000) have shown that their values are overestimated by a factor of 2, on average. The coronal properties determined for cluster members are typical of highly active stars. Multi-temperature models with at least two components were needed in the model-fitting. In the cases in which flare-like events were detected, a third hotter component was necessary to account for the enhancement of hard X-ray emission. In general, the stars that underwent a flare during our observations showed enhanced pseudo-quiescent X-ray luminosities with respect to members with similar spectral type that showed no flares. Six flares were detected in five of the cluster members, with energies that are typical of pre-main- and main-sequence M stars. For these stars, coronal properties and X-ray luminosities were determined for the flare and the pseudo-quiescent states.

From the comparison of the X-ray luminosity of cluster members in different environments: the presence or not of a protoplanetary disk in different evolutionary stages and binarity, we concluded that the only parameter that seems to influence the overall X-ray emission of the stars in $\eta$ Chamaleontis is the spectral type. A similar conclusion may be extracted for the flare energies, although the sample of flare-like events during our observations is too poor to achieve a robust conclusion.

To complete our study, we searched for other cluster members in the field-of-view that could had gone unnoticed in previous surveys. We found five candidates, but discarded them as cluster members after a detailed study of their optical spectroscopic properties.

*Acknowledgements.* J.L-S. and M.A.L-G. acknowledge support by the Spanish Ministerio de Ciencia e Innovación under grant AYA2008-06423-C03-03. J.F.A.C., is researcher of the CONICET and acknowledges support by grant PICT 2007-02177 (SecyT). We would like to acknowledge the anonymous referee for his/her useful comments on the text content.

## References

Alecian, E., Catala, C., van't Veer-Menneret, C., Goupil, M.-J., & Balona, L. 2005, A&A, 442, 993

Arnaud, K. 1996, XSPEC: The First Ten Years. In ASP Conf. Ser. 101, eds. George H. Jacoby and Jeannette Barnes, 17
Arnaud, K. 2004, XSPEC: Progress and Plans. In the American Astronomical Society, HEAD meeting 8, 16.29
Baraffe, I., Chabrier, G., Allard, F., & Hauschildt, P. H. 1998, A&A, 337, 403
Böhm, T., Zima, W., Catala, C., Alecian, E., Pollard, K., & Wright, D. 2009, A&A, 497, 183
Brickhouse, N. S., Cranmer, S. R., Dupree, A. K., Luna, G. J. M., & Wolk, S. 2010, ApJ, 710, 1835
Briggs, K. R., & Pye, J. P. 2003, MNRAS, 345, 714
Buscombe, W., & Morris, P. M. 1961, MNRAS, 123, 233
Caballero, J. A., López-Santiago, J., de Castro, E., & Cornide, M. 2009, AJ, 137, 5012
Caballero, J. A., Albacete Colombo, J. A., & López-Santiago, J. 2010, A&A(in press; arXiv:1006.4115)
Clausen, J. V., & Nordstrom, B. 1980, A&A, 83, 339
Crespo-Chacón, I., Micela, G., Reale, F., Caramazza, M., López-Santiago, J., & Pillitteri, I. 2007, A&A, 471, 929
Damiani, F., Maggio, A., Micela, G., & Sciortino, S. 1997, ApJ, 483, 350
Della Ceca, R., et al. 2004, A&A, 428, 383
Favata, F., Flaccomio, E., Reale, F., Micela, G., Sciortino, S., Shang, H., Stassun, K. G., & Feigelson, E. D. 2005, ApJS, 160, 469
Flaccomio, E., Micela, G., Sciortino, S., Feigelson, E. D., Herbst, W., Favata, F., Harnden, F. R., Jr., & Vrtilek, S. D. 2005, ApJS, 160, 450
Franciosini, E., Pillitteri, I.; Stelzer, B., Micela, G., Briggs, K. R., Scelsi, L., Telleschi, A., Audard, M., Palla, F., & Gdel, M. 2007, A&A, 468, 485
Frink, S., Roeser, S., Alcala, J. M., Covino, E., & Brandner, W. 1998, A&A, 338, 442
Gómez de Castro, A. I. 2009, ApJ, 698, L108
Güdel, M., et al. 2007, A&A, 468, 353
Guenther, E. W., Esposito, M., Mundt, R., Covino, E., Alcalá, J. M., Cusano, F., & Stecklum, B. 2007, A&A, 467, 1147
Haisch, K. E., Jr., Jayawardhana, R., & Alves, J. 2005, ApJ, 627, L57
Köhler, R., & Petr-Gotzens, M. G. 2002, AJ, 124, 2899
Lawson, W. A., Crause, L. A., Mamajek, E. E., & Feigelson, E. D. 2002, MNRAS, 329, L29
López-Santiago, J., Micela, G., Sciortino, S., Favata, F., Caccianiga, A., Della Ceca, R., Severgnini, P., & Braito, V. 2007, A&A, 463, 165
López-Santiago, J., & Caballero, J. A. 2008, A&A, 491, 961
López-Santiago, J., Crespo-Chacón, I., Micela, G., & Reale, F. 2010, ApJ, 712, 78
Luhman, K. L. 2004, ApJ, 616, 1033
Lyo, A.-R., Lawson, W. A., Mamajek, E. E., Feigelson, E. D., Sung, E.-C., & Crause, L. A. 2003, MNRAS, 338, 616
Lyo, A.-R., Lawson, W. A., Feigelson, E. D., & Crause, L. A. 2004, MNRAS, 347, 246
Lyo, A.-R., Song, I., Lawson, W. A., Bessell, M. S., & Zuckerman, B. 2006, MNRAS, 368, 1451
Mamajek, E. E., Lawson, W. A., & Feigelson, E. D. 1999, ApJ, 516, L77
Mamajek, E. E., Lawson, W. A., & Feigelson, E. D. 2000, ApJ, 544, 356
Marconi, M., & Palla, F. 1998, ApJ, 507, L141
Marino, A., Micela, G., Peres, G., & Sciortino, S. 2003, A&A, 406, 629
Megeath, S. T., Hartmann, L., Luhman, K. L., & Fazio, G. G. 2005, ApJ, 634, L113
Moraux, E., Lawson, W. A., & Clarke, C. 2007, A&A, 473, 163
Morrison, R., & McCammon, D. 1983, ApJ, 270, 119
Murphy, S. J., Lawson, W. L., & Bessel, M. S. 2010, MNRAS (in press), arXiv:1005.3308
Preibisch, T., et al. 2005, ApJS, 160, 401
Robrade, J., & Schmitt, J. H. M. M 2005, A&A, 435, 1073
Sacco, G. G., Argiroffi, C., Orlando, S., Maggio, A., Peres, G., & Reale, F. 2008, A&A, 491, L17
Sicilia-Aguilar, A., et al. 2009, ApJ, 701, 1188
Siess, L., Dufour, E., & Forestini, M. 2000, A&A, 358, 593
Schmitt, J. H. M. M., Collura, A., Sciortino, S., Vaiana, G. S., Harnden, F. R., Jr., & Rosner, R. 1990, ApJ, 365, 704
Skrutskie, M. F., et al. 2006, AJ, 131, 1163
Smith, R. K., Brickhouse, N. S., Liedahl, D. A., & Raymond, J. C. 2001a, ApJ, 556, L91
Smith, R. K., Brickhouse, N. S., Liedahl, D. A., & Raymond, J. C. 2001b, ASP Conf. Ser. 247: Spectroscopic Challenges of Photoionized Plasmas, 247, 161
Song, I., Zuckerman, B., & Bessell, M. S. 2004, ApJ, 600, 1016
Stelzer, B., Micela, G., Hamaguchi, K., & Schmitt, J. H. M. M. 2006, A&A, 457, 223
Stelzer, B., Flaccomio, E., Briggs, K., Micela, G., Scelsi, L., Audard, M., Pillitteri, I., Guedel, M. 2007, A&A, 468, 463
Stelzer, B., Robrade, J., Schmitt, J. H. M. M., & Bouvier, J. 2009, A&A, 493, 1109
Torres, C. A. O., Quast, G. R., Melo, C. H. F., & Sterzik, M. F. 2008, Handbook of Star Forming Regions, Volume II, 757

## Appendix A: On-line material

**Table A.1.** Sources detected in the 0.3–7.5 keV energy band using PWDetect with detection threshold $SNR = 5$.

| Src # | Right Ascension (h m s) | Declination (° ′ ″) | Significance | Count-rate ($\times10^{-3}$ s$^{-1}$) | Observed flux* ($\times10^{-13}$ erg cm$^{-2}$ s$^{-1}$) | Notes |
|---|---|---|---|---|---|---|
| 1 | 08 45 33.9 | -79 13 33.5 | 6.0 | 1.3 ± 0.7 | 0.09 ± 0.05 | |
| 2 | 08 42 42.8 | -79 10 59.3 | 5.8 | 1.9 ± 0.3 | 0.14 ± 0.03 | |
| 3 | 08 44 07.3 | -79 10 13.1 | 6.1 | 1.1 ± 0.2 | 0.08 ± 0.02 | |
| 4 | 08 43 19.7 | -79 09 50.1 | 6.6 | 0.9 ± 0.2 | 0.07 ± 0.02 | |
| 5 | 08 40 53.4 | -79 09 03.9 | 6.5 | 3.8 ± 0.4 | 0.29 ± 0.05 | |
| 6 | 08 45 42.3 | -79 07 11.7 | 7.0 | 0.6 ± 0.1 | 0.04 ± 0.01 | |
| 7 | 08 44 9.4 | -79 06 17.8 | 5.9 | 0.6 ± 0.1 | 0.04 ± 0.01 | 2MASS J08440921-7906156, field giant |
| 8 | 08 42 10.8 | -79 06 02.3 | 5.8 | 0.3 ± 0.1 | 0.02 ± 0.01 | |
| 9 | 08 43 18.4 | -79 05 20.2 | 14.0 | 1.4 ± 0.2 | 0.10 ± 0.02 | RECX 15 |
| 10 | 08 41 30.5 | -79 05 02.9 | 8.1 | 0.7 ± 0.2 | 0.05 ± 0.01 | |
| 11 | 08 49 20.9 | -79 04 50.9 | 5.6 | 1.0 ± 0.6 | 0.08 ± 0.05 | |
| 12 | 08 43 07.7 | -79 04 53.9 | 244.9 | 131.9 ± 1.6 | 9.86 ± 1.32 | RECX 7 |
| 13 | 08 42 49.6 | -79 04 31.4 | 5.3 | 0.5 ± 0.1 | 0.03 ± 0.01 | |
| 14 | 08 43 12.5 | -79 04 13.3 | 140.1 | 45.7 ± 1.0 | 3.41 ± 0.46 | RECX 8 |
| 15 | 08 43 18.0 | -79 04 10.6 | 5.7 | 0.3 ± 0.2 | 0.02 ± 0.02 | |
| 16 | 08 42 24.2 | -79 04 04.6 | 170.4 | 67.3 ± 1.2 | 5.03 ± 0.68 | RECX 4 |
| 17 | 08 47 15.0 | -79 03 55.0 | 6.1 | 1.5 ± 0.2 | 0.12 ± 0.02 | |
| 18 | 08 41 37.2 | -79 03 31.3 | 43.2 | 10.3 ± 0.5 | 0.77 ± 0.11 | RECX 3 |
| 19 | 08 45 50.4 | -79 02 58.0 | 7.2 | 0.5 ± 0.1 | 0.04 ± 0.01 | |
| 20 | 08 45 47.8 | -79 02 38.4 | 6.1 | 0.2 ± 0.1 | 0.02 ± 0.01 | |
| 21 | 08 45 13.8 | -79 02 37.2 | 9.9 | 0.8 ± 0.1 | 0.06 ± 0.01 | |
| 22 | 08 41 22.7 | -79 02 33.0 | 6.9 | 0.9 ± 0.2 | 0.07 ± 0.02 | |
| 23 | 08 43 31.6 | -79 02 08.3 | 14.0 | 1.0 ± 0.1 | 0.08 ± 0.01 | |
| 24 | 08 48 10.6 | -79 01 05.9 | 8.7 | 1.5 ± 0.2 | 0.11 ± 0.02 | |
| 25 | 08 41 39.9 | -79 00 55.7 | 5.5 | 0.2 ± 0.1 | 0.01 ± 0.01 | |
| 26 | 08 40 32.8 | -79 00 45.8 | 5.7 | 0.7 ± 0.1 | 0.05 ± 0.01 | |
| 27 | 08 46 55.5 | -79 00 17.7 | 5.1 | 0.3 ± 0.1 | 0.02 ± 0.01 | |
| 28 | 08 40 24.1 | -79 00 12.0 | 5.7 | 0.6 ± 0.1 | 0.05 ± 0.01 | |
| 29 | 08 47 01.8 | -79 00 11.4 | 5.8 | 0.4 ± 0.1 | 0.03 ± 0.01 | |
| 30 | 08 39 47.2 | -79 00 04.6 | 11.2 | 2.0 ± 0.2 | 0.15 ± 0.03 | 2MASS J08394669-7900026, AGN |
| 31 | 08 45 05.3 | -79 00 09.3 | 16.9 | 1.3 ± 0.1 | 0.10 ± 0.02 | |
| 32 | 08 46 02.6 | -79 00 01.0 | 7.7 | 0.6 ± 0.1 | 0.05 ± 0.01 | |
| 33 | 08 46 20.8 | -78 59 58.2 | 6.0 | 0.5 ± 0.2 | 0.04 ± 0.02 | |
| 34 | 08 47 02.4 | -78 59 36.5 | 320.1 | 251.6 ± 2.0 | 18.81 ± 2.51 | RECX 11 |
| 35 | 08 41 36.3 | -78 59 34.3 | 6.5 | 0.6 ± 0.1 | 0.04 ± 0.01 | |
| 36 | 08 43 20.7 | -78 59 34.9 | 13.7 | 0.7 ± 0.1 | 0.05 ± 0.01 | |
| 37 | 08 44 17.1 | -78 59 10.0 | 149.4 | 31.1 ± 0.5 | 2.33 ± 0.31 | RECX 9 |
| 38 | 08 46 56.9 | -78 58 55.5 | 5.8 | 0.4 ± 0.1 | 0.03 ± 0.01 | |
| 39 | 08 40 29.4 | -78 58 41.0 | 15.4 | 2.9 ± 0.3 | 0.21 ± 0.04 | |
| 40 | 08 41 38.3 | -78 58 41.3 | 32.2 | 5.3 ± 0.3 | 0.40 ± 0.06 | |
| 41 | 08 44 54.4 | -78 58 38.6 | 12.1 | 0.6 ± 0.1 | 0.05 ± 0.01 | |
| 42 | 08 40 34.5 | -78 58 31.4 | 10.6 | 1.0 ± 0.2 | 0.08 ± 0.02 | |
| 43 | 08 43 36.7 | -78 58 29.4 | 6.9 | 0.3 ± 0.1 | 0.02 ± 0.01 | |
| 44 | 08 44 25.5 | -78 58 18.9 | 14.5 | 1.1 ± 0.1 | 0.08 ± 0.01 | |
| 45 | 08 44 06.7 | -78 57 53.4 | 21.2 | 3.1 ± 0.2 | 0.23 ± 0.03 | |
| 46 | 08 42 27.6 | -78 57 49.5 | 58.7 | 8.3 ± 0.3 | 0.62 ± 0.09 | RECX 5 |
| 47 | 08 43 24.5 | -78 56 46.1 | 15.8 | 1.0 ± 0.1 | 0.07 ± 0.01 | |
| 48 | 08 43 36.1 | -78 56 32.7 | 5.4 | 0.1 ± 0.0 | 0.01 ± 0.00 | |
| 49 | 08 41 09.0 | -78 56 01.0 | 7.8 | 0.8 ± 0.1 | 0.06 ± 0.01 | |
| 50 | 08 49 01.1 | -78 55 52.3 | 22.3 | 8.2 ± 1.3 | 0.62 ± 0.13 | |
| 51 | 08 44 42.3 | -78 55 51.2 | 7.9 | 0.6 ± 0.1 | 0.04 ± 0.01 | |
| 52 | 08 43 39.0 | -78 55 41.4 | 23.6 | 2.1 ± 0.2 | 0.16 ± 0.02 | |
| 53 | 08 45 36.0 | -78 55 35.8 | 6.2 | 0.6 ± 0.1 | 0.05 ± 0.01 | |
| 54 | 08 48 01.1 | -78 55 20.0 | 7.8 | 0.9 ± 0.2 | 0.07 ± 0.02 | |
| 55 | 08 47 57.4 | -78 54 52.9 | 128.4 | 167.2 ± 1.7 | 12.50 ± 1.67 | RECX 12 |
| 56 | 08 48 35.9 | -78 54 50.0 | 10.7 | 2.3 ± 0.3 | 0.17 ± 0.03 | |
| 57 | 08 41 20.2 | -78 54 49.4 | 7.9 | 1.6 ± 0.1 | 0.12 ± 0.02 | |
| 58 | 08 40 20.3 | -78 54 42.3 | 11.1 | 3.6 ± 0.3 | 0.27 ± 0.04 | |
| 59 | 08 42 39.3 | -78 54 43.7 | 116.1 | 27.0 ± 0.6 | 2.02 ± 0.27 | RECX 6 |
| 60 | 08 45 19.6 | -78 54 43.8 | 10.7 | 0.9 ± 0.2 | 0.07 ± 0.02 | |
| 61 | 08 45 01.9 | -78 54 40.4 | 11.9 | 1.0 ± 0.1 | 0.08 ± 0.01 | |
| 62 | 08 47 52.2 | -78 54 16.4 | 6.2 | 0.5 ± 0.1 | 0.03 ± 0.01 | |
| 63 | 08 43 13.7 | -78 54 14.5 | 6.5 | 0.5 ± 0.1 | 0.04 ± 0.01 | |
| 64 | 08 44 29.9 | -78 54 03.5 | 5.3 | 0.2 ± 0.0 | 0.01 ± 0.00 | |
| 65 | 08 48 35.4 | -78 53 48.4 | 5.9 | 1.6 ± 0.4 | 0.12 ± 0.04 | 2MASS J08483486-7853513, field dM5e |
| 66 | 08 43 16.6 | -78 53 44.1 | 7.6 | 0.5 ± 0.1 | 0.03 ± 0.01 | 2MASS J08431595-7853422, field M |
| 67 | 08 43 33.4 | -78 53 24.0 | 24.2 | 2.6 ± 0.2 | 0.19 ± 0.03 | |
| 68 | 08 39 47.4 | -78 53 01.4 | 36.2 | 22.5 ± 11.3 | 1.68 ± 0.88 | |
| 69 | 08 41 29.9 | -78 53 05.2 | 5.1 | 0.6 ± 0.1 | 0.04 ± 0.01 | RECX 14 |
| 70 | 08 45 08.9 | -78 53 03.5 | 5.7 | 0.2 ± 0.1 | 0.02 ± 0.00 | |
| 71 | 08 45 39.8 | -78 52 58.3 | 8.4 | 1.1 ± 0.2 | 0.08 ± 0.02 | |
| 72 | 08 41 43.0 | -78 52 42.9 | 12.5 | 1.4 ± 0.2 | 0.11 ± 0.02 | |
| 73 | 08 41 26.1 | -78 52 16.5 | 11.5 | 1.2 ± 0.2 | 0.09 ± 0.02 | |
| 74 | 08 47 39.1 | -78 50 36.0 | 6.8 | 1.2 ± 0.2 | 0.09 ± 0.02 | |
| 75 | 08 47 52.1 | -78 50 10.4 | 8.2 | 0.8 ± 0.2 | 0.06 ± 0.01 | |
| 76 | 08 45 18.5 | -78 49 40.9 | 5.7 | 0.9 ± 0.2 | 0.07 ± 0.02 | |
| 77 | 08 44 54.2 | -78 48 36.9 | 9.9 | 1.1 ± 0.2 | 0.08 ± 0.02 | |
| 78 | 08 45 04.5 | -78 48 28.3 | 14.4 | 3.1 ± 0.3 | 0.23 ± 0.04 | |
| 79 | 08 43 37.7 | -78 48 25.5 | 8.0 | 0.8 ± 0.2 | 0.06 ± 0.01 | |
| 80 | 08 44 59.8 | -78 48 15.8 | 11.7 | 2.1 ± 0.3 | 0.16 ± 0.03 | |
| 81 | 08 43 32.2 | -78 48 13.4 | 10.6 | 0.9 ± 0.2 | 0.07 ± 0.01 | |
| 82 | 08 45 53.2 | -78 47 59.2 | 7.4 | 2.3 ± 0.3 | 0.17 ± 0.03 | |
| 83 | 08 46 14.0 | -78 47 39.0 | 5.4 | 1.0 ± 0.2 | 0.07 ± 0.02 | |
| 84 | 08 45 23.7 | -78 47 23.8 | 11.3 | 2.6 ± 0.3 | 0.19 ± 0.03 | |
| 85 | 08 44 32.2 | -78 46 31.7 | 88.5 | 41.3 ± 1.4 | 3.09 ± 0.42 | RECX 10 |
| 86 | 08 45 27.8 | -78 45 45.4 | 5.7 | 1.0 ± 0.2 | 0.07 ± 0.02 | |

**Notes.** (*) Observed fluxes determined using the conversion factor $CF = 1.5 \pm 0.2 \times 10^{-9}$ erg ph$^{-1}$. Fluxes from the spectral fitting for the known cluster members are given in Table 2.

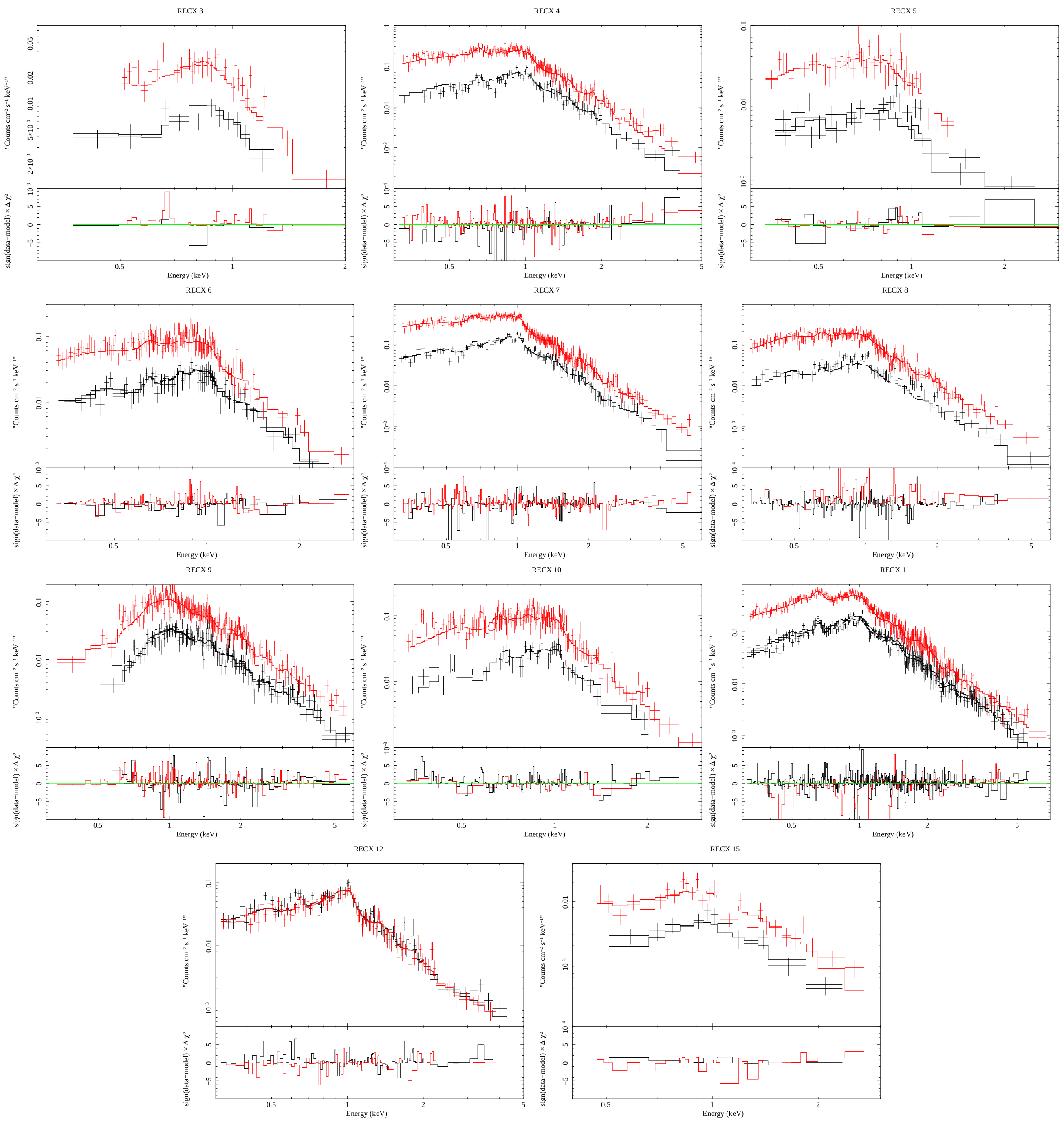

**Fig. A.1.** X-ray spectra for known members of $\eta$ Chamaleontis. Red is for EPIC-pn and black is for EPIC-mos, except for RECX 12 that is located in an EPIC-pn gap. The best fit to each spectrum is also plotted. The bottom panel represents the deviation of the model from the observed spectra in each spectral bin.

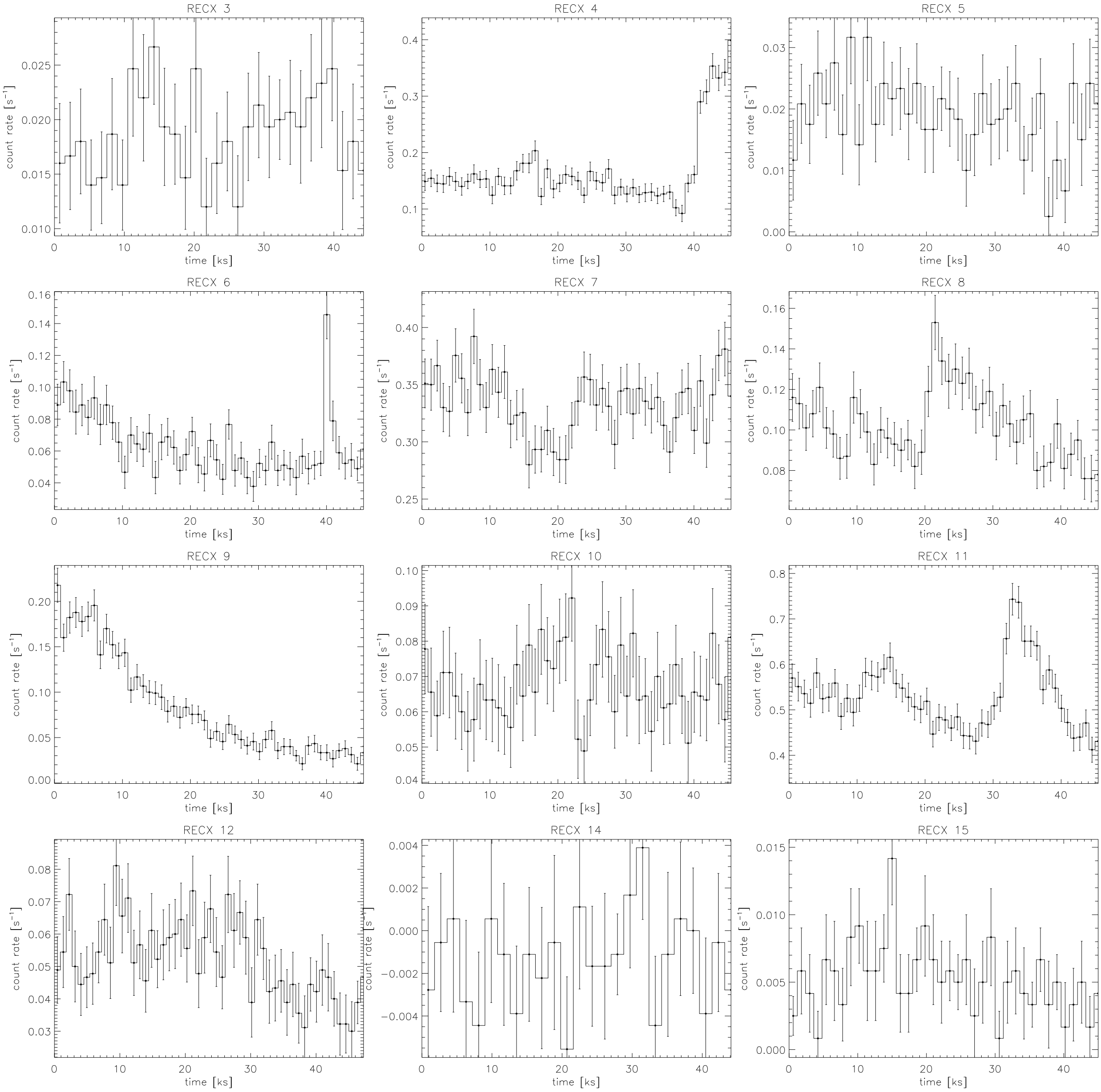

**Fig. A.2.** X-ray light curves in the energy band 0.3–8.0 keV for known members of $\eta$ Chamaleontis. Time binning ranges from 15 to 30 minutes.